Journal Pre-proof

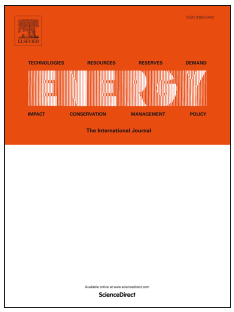

Advanced methodology for wind resource assessment near hydroelectric dams in complex mountainous areas

Lin Yang, Jose I. Rojas, Adeline Montlaur

PII: S0360-5442(19)32182-6

DOI: https://doi.org/10.1016/j.energy.2019.116487

Reference: EGY 116487

To appear in: *Energy*

Received Date: 6 February 2019

Revised Date: 22 October 2019

Accepted Date: 3 November 2019

Please cite this article as: Yang L, Rojas JI, Montlaur A, Advanced methodology for wind resource assessment near hydroelectric dams in complex mountainous areas, *Energy* (2019), doi: https://doi.org/10.1016/j.energy.2019.116487.

Advanced methodology for wind resource assessment near hydroelectric dams in complex mountainous areas

Lin Yang[a, *], Jose I. Rojas[b], Adeline Montlaur[b, c]

[a] School of Engineering, RMIT University, PO Box 71, Bundoora, VIC 3083, Australia

[b] Department of Physics – Division of Aerospace Engineering, Universitat Politècnica de Catalunya; c/ Esteve Terradas 7, 08860, Castelldefels, Spain

[c] Laboratori de Càlcul Numèric, Universitat Politècnica de Catalunya; Jordi Girona 1, E-08034 Barcelona, Spain

* Corresponding author, email: lin.yang@student.rmit.edu.au

Abstract

To increase renewable energy generation in some hydroelectric dams, a solution consisting in installing wind turbines close to dams is proposed. Indeed, dam surroundings are prone to benefit from wind speed-up effect, extra wind generation associated with thermal winds, and existing electrical infrastructure. Identifying the most suitable locations for turbines, that is, areas of relatively high-speed and low-turbulence wind, is fundamental to maximize this complementary power. Easy accessibility to turbines and minimum distance to dam electrical infrastructure are also essential to reduce the costs. Thus, a methodology is proposed to improve wind resource assessment in complex mountainous areas. First, potentially interesting dams are chosen using statistical local wind data. Second, weighted results of wind speed and turbulence intensity, considering all wind directions are presented based on CFD simulations. Finally, wind power density and annual energy production maps are generated, along with accessibility maps, to identify suitable sites. The Camarasa dam in the north-east of the Iberian Peninsula is chosen as case study to show and test the proposed methodology. Error estimations are provided, along with validation against Wind Atlas data and WAsP simulations.

Keywords: Wind energy; power density; wind turbine; hydroelectric dam; CFD

1. Introduction

In recent years, many studies have suggested a future increase of temperature and decrease of annual rainfall in areas of Mediterranean climate as a consequence of global warming [1, 2]. These trends are confirmed by on-site observations [3]. These changes are expected to be more intense over land than over sea. Thus, these areas will suffer a decrease in water resources [4] and water stored in reservoirs [2, 5]. Consequently, uses of this water may have to be modified. Namely, there

will be constraints on hydropower, since water will have to be saved for irrigation of crops and human consumption, as in Spain in 2017 due to generalized draught. A global temperature warming of 3ºC could cause reductions of hydropower by 15–20% in countries like Greece, Portugal, and Spain [6]. Meanwhile, the global demand of electricity continues to increase along with the development of society [7]. Thus, a complementary solution for renewable energy generation in the current hydroelectric system arises interest.

Moreover, projections of wind energy density (WED) in Europe for the 21st century reveal a likely increase of mean annual WED over Northern and Central Europe, but a likely decrease over Southern Europe [8, 9], due to a likely decrease in intensity of synoptic or atmospheric boundary layer (ABL) winds. A stronger decadal variability [10] and intra-annual variability of WED over most of Europe is also predicted, and thus higher irregularity of wind energy production [8], making more difficult the fit of wind energy in the market. A WED decrease in mid latitudes of the Northern hemisphere is suggested also in [11]; in Portugal, wind power may decrease 10–20% in winter and spring, and 25–35% in autumn [12]. Thus, it is important to explore wind resources associated with other regimes such as thermal winds, which show higher regularity and periodicity [13].

Considering that most dams are built in valleys and mountainous areas, where thermal winds usually arise [14], a solution to help counterbalancing the likely hydropower decrease would consist in installing wind turbines nearby. Thermal winds generated in mountainous areas could be sufficient to drive small/medium turbines [15], as confirmed using typical mountain slopes and temperature gradients of the Pyrenees mountain range [16] in katabatic wind models [17]. Moreover, mountainous surroundings of dams are prone to show wind speed-up effect, which would increase turbine capacity factor. Another important benefit is that turbines located near hydroelectric dams would take advantage of existing infrastructure for electricity handling and distribution. Since the cost of building electricity networks accounts for ≈12% of the total wind farm cost [18], this could save construction costs compared with isolated farms. Finally, in protected mountainous areas, installing turbines near dams may help circumvent possible restrictions.

The topography around dams is usually complex and variable. To easily install and maintain turbines, the selected sites should be easily accessible [19]. Ideally, the sites should be close to the dam to minimize the cost of reusing the available electric infrastructure, since building small power transmission lines costs ≈190 k€/km [20]. Wind shear should also be taken into account, since uniform incident wind speed profile is required for higher performance and service life of the turbines, while thermal winds may show significant wind shear. Furthermore, the speed-up phenomenon over topography has long been recognized as significant for structural design and wind

energy applications. Investigations have been made on understanding the flow to obtain information such as the maximum value of mean and gust speed-up and the extent of the accelerated flow region [21, 22]. In mountainous areas, the speed-up effect is thus critical for turbine sitting.

Several approaches for wind resource assessment and turbine sitting have been developed. Namely, extrapolating wind data from nearby weather stations using linear microscale models like Wind Atlas Analysis and Application Program (WAsP) [23]. Alternatively, a downscaling process based on tools like the Global Wind Atlas (GWA) [24]. Here, Numerical Weather Prediction (NWP) models are used to estimate the wind resource over large regions, based on satellite observations [25]. Then, these data are reanalyzed for mesoscale modelling, which downscales the data into medium scale [26]. Finally, further downscaling can be achieved by using linear microscale models [27]. Although linear equations (used in the above approaches) may not always be accurate for evaluating wind behaviour over complex terrains, e.g., hills, steep mountains, and valleys [28], they have often proven to be valid [29, 30].

The challenge for wind resource estimation in complex terrains is to capture the main features of the wind, while keeping the computational effort at an acceptable level, by concentrating on the details of the flow pertinent to wind energy issues [31]. Though being resource consuming, Computational Fluid Dynamics (CFD) has proven valuable for wind energy applications on ground and offshore [32, 33], and particularly for modelling wind over complex terrains by using non-linear models, including the Navier-Stokes equations [23]. The output of CFD simulations, providing information on, e.g., wind speed, turbulence, and potential power production over the whole region of interest [34], can help identify suitable sites and hub-heights for turbines. Thus, results can be visualized for wind resource assessment and turbine sitting [35].

Recently, several CFD analyses of wind over complex terrains have been performed, studying the effect of terrain size, surface roughness, ABL, and forests on CFD predictions [36, 37]. Moreover, different turbulence models including Large-Eddy Simulation (LES) have been tested [38], and turbine wake effects on wind farms have been analyzed [39]. Besides general CFD software, special CFD software for wind farm design, like WindSim and Meteodyn, have been tested and adopted for wind resource assessment [19, 29, 40, 41]. To improve accuracy, a method was proposed that corrects CFD results by means of coupling with data from multiple surrounding masts [42].

The objective of this work is to propose an easy-to-follow methodology to assess the wind resource in complex terrains like areas surrounding dams, using wind data from weather stations and/or other sources like GWA, as well as statistical analyses and CFD simulations. The goal is also to raise attention and facilitate preliminary feasibility analyses on a complementary solution for renewable

energy generation, consisting in installing turbines close to hydropower dams. Since in complex terrains, like near dams, linearly-calculated predictions might show error with respect to the real flow, we test a linear approach, evaluating the error, and results are compared with those from GWA and WAsP simulations. We thus aim to contribute to the ongoing discussion in the literature about whether linear equations are suitable to model wind behaviour over complex terrains. Moreover, most studies only consider annual mean wind speeds, whereas in this work uncertainty is assessed by considering annual wind direction distributions in 16 direction bins. Finally, most previous studies focused on isolated hills, except works on isolated islands [19, 35] and marine channels [43]. Thus, no similar work has been done combining statistical analyses and CFD simulations of wind energy in areas near dams, where speed-up effects and thermal winds are important factors, which are not always easy to detect.

The proposed procedure for turbine sitting, applicable to any dam, is depicted in Section 2. Then, it is further detailed through a specific case study in Section 3, where results are compared with those from conventional WAsP simulations, and finally the conclusions are drawn in Section 4.

2. Proposed methodology

In this work, a global methodology to assess the wind resource near dams and to decide the best sites for turbine sitting is described. Figure 1 and this section briefly summarize the main steps, which will be commented with further detail through the case study in Section 3.

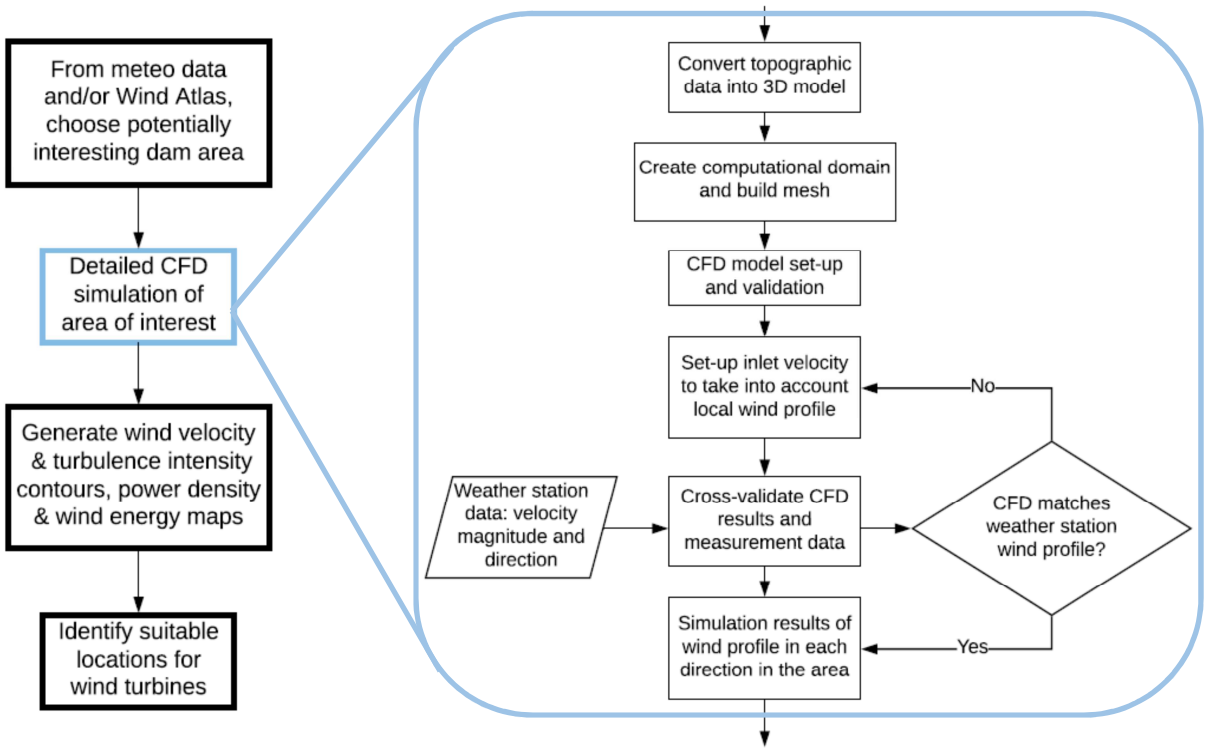

Figure 1. Flow chart of the proposed wind resource assessment procedure

2.1 Identifying potentially interesting areas

To assess the viability of installing turbines near dams, a statistical study of the local wind in these regions should first be performed. Note that such data can be obtained from local weather stations, from national weather agencies, or from a myriad of weather data sources, such as the National Oceanic and Atmospheric Administration (NOAA) or GWA. Figure 2 shows examples of wind roses obtained thanks to a local weather station (left) and to GWA (right).

Once statistically-relevant data are obtained (several years of measurement should be considered), there are several methods to obtain the wind power and energy produced [44]. The static method, widely used by the wind energy industry for preliminary wind power analysis [45, 46], is the simplest one, as it ignores non-stationary effects, such as changes in wind direction and turbine maintenance periods. The method is based on the principle that the probability density function of the power produced follows a two-parameter Weibull function with the same scale and shape factors as the Weibull function corresponding to the wind speed distribution the power originated from. That is, both probability distributions are two identical Weibull curves, which can be expressed as:

$$f(V) = \left(\frac{k}{\lambda}\right)\left(\frac{V}{\lambda}\right)^{k-1} e^{-\left(\frac{V}{\lambda}\right)^{k}} \qquad (V > 0;\ k, \lambda > 0) \tag{1}$$

where $f(V)$ is the probability of observing a given wind speed V, λ is the scale parameter, and k is the dimensionless shape parameter.

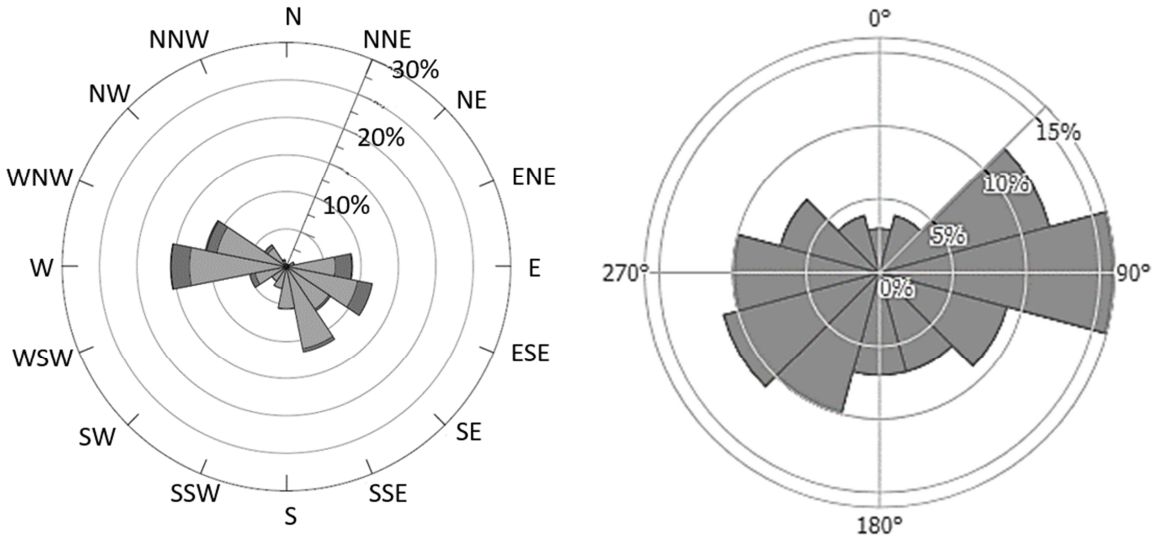

Figure 2. Wind rose in Camarasa: (left) from MeteoCat weather station data at 2 m AGL; (right) from Global Wind Atlas (GWA) data at 50 m AGL on a 10 × 10 km^2 around Camarasa (DTU, 2018)

After that, following the static method, the probability for a turbine to generate a given output power is obtained by combining the Weibull distribution of the wind speed and the turbine power curve. Particularly, if ρ is the air density, the wind power density (WPD) can be calculated as follows:

$$\frac{P}{V} = \frac{1}{2}\rho\lambda^3\Gamma\left(1+\frac{3}{k}\right) \quad (2)$$

Comparing the WPD in several locations of interest will give a preliminary estimation of the available wind power in the area, and will allow to delimitate the area of highest interest for wind turbine sittings. Another interesting factor for the choice of the location could be to assess if the site is prone to develop thermal winds or not, since interestingly these are more regular than synoptic winds. More details on this part will be given in Section 3.1.

2.2 CFD simulation of the area of interest

Once the area of interest has been identified, the CFD process can start. First, a topographic model must be created, and then meshed. Second, CFD simulations are set up. The methodology proposed here is independent of the CFD method or software chosen. In the selected case study, we used ANSYS ICEM CFD 17.2 software, but obviously open-source CFD software, such as OpenFOAM, could also be used to make the proposed methodology even more affordable to any interested institution.

In any case, some common hypotheses will have to be made. Namely, a logarithmic wind profile law:

$$V_H = V_{ref}\frac{ln(H/Z_0)}{ln(H_{ref}/Z_0)} \quad (3)$$

can be defined at the inlet of the computational domain, where H is the altitude above ground level (AGL), V_H is the wind speed at height H, V_{ref} is the wind speed measured at reference height H_{ref}, and z_0 is the roughness length.

A tuning of the inlet velocity can be performed to assess how the local wind direction and speed change from the ones imposed at the inlet of the domain. More details on this part will be given in Section 3.3.

If statistical data are available at specific locations, for example from weather stations, mean wind profiles should be available for several wind directions, each corresponding to a given weighting factor, as shown for example in Figure 2 (left). CFD simulations and analyses should thus be conducted for all wind scenarios, or at least the most habitual ones. Afterwards, the final wind

profiles can be analysed by post-processing all simulation results and by considering the weighting factor of each wind direction.

Results of this CFD study would consist in wind velocity maps for different wind directions, maps of weighted average of wind speed and turbulence kinetic energy (TKE), etc.

2.3 Post-processing of power density and wind energy maps

To complete the CFD results, detailed distributions of wind (both in magnitude and direction) along the year can be computed following a series of steps. After studying the effects of non-linearity of the CFD simulations, linearity is assumed at this stage to generate global maps of WPD. These maps take into account the detail of wind direction in the calculation of WPD and energy, leading to more accurate results than if wind direction is not taken into account. After choosing a specific model of wind turbine, maps of annual wind energy production can also be generated. Details of this step are found in Section 3.5.

2.4 Identifying suitable locations

The proposed methodology aims to identify suitable sites for wind turbines based on four criteria:

1. the site should be easily accessible (to limit the cost of installation and maintenance of the turbines)
2. given that the locations are in mountainous areas, the site should take advantage of the speed-up effect (to maximise the energy production of the turbine)
3. uniform incident wind speed profiles should be observed locally (to maximize wind turbine efficiency)
4. the site should be close to its pairing hydropower dam (to limit the electric grid connection costs)

The proposed methodology provides relevant information to the decision-maker about these four criteria for turbine sitting. Note that, complementary criteria, such as a thorough study of economic feasibility, could also be taken into account, but this is considered to be out of the scope of this work, since it would involve a multiplicity of factors very specific of each country and location.

3. Case study: Camarasa dam

The proposed methodology is detailed and tested through a particular case study, but it is important to recall that it is applicable to any region of interest near dams.

3.1 Identification and description of potentially interesting areas

Four mountainous regions of Catalunya (Spain) were chosen as possible candidates for wind resource assessment (see Figure 3). Darnius Boadella, Certascan, Camarasa, and Oliana dams are found in each of these areas, storing water and generating hydropower. Weather stations of the *Catalan Weather Service* (MeteoCat) are located close to these dams, measuring local wind speed and direction [47].

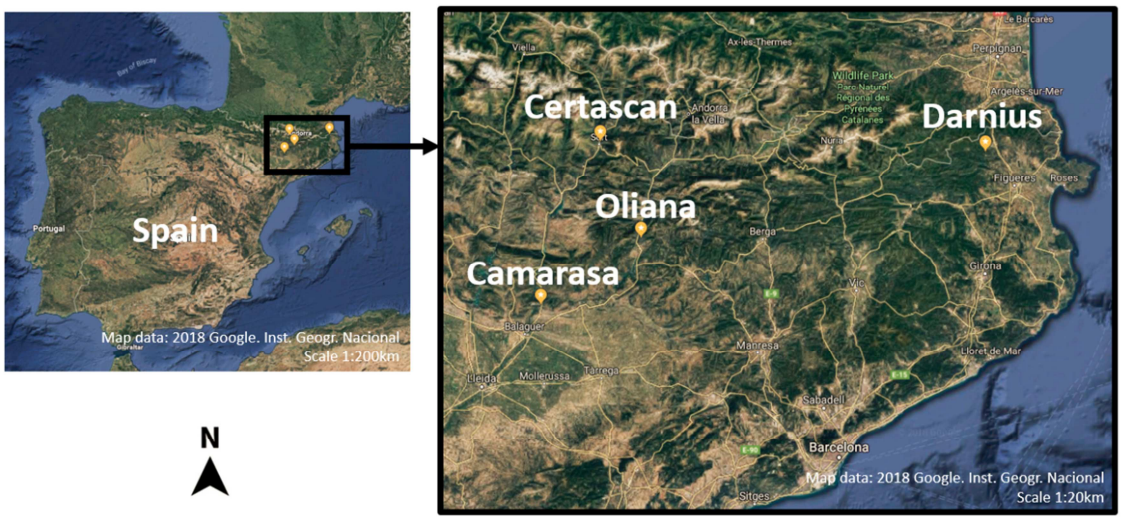

Figure 3. Four candidate dams in Catalunya, NE of the Iberian Peninsula

Based on the wind speed data collected from the weather stations and using Eq. (1) , it was found that Weibull distributions fit well the data in these four locations. The distributions were validated using the two-sample Kolmogorov-Smirnov test at significant level of 0.05. The WPD Eq. (2) was then applied, and Table 1 shows the results obtained from this analysis for the mean wind speed, standard deviation, and WPD at 10 m AGL, for each weather station. The highest WPD corresponds to Camarasa, which is thus selected for conducting the subsequent case study.

Table 1. Statistical analysis of wind speed at 10 m AGL from weather station measurements close to candidate dams

	Mean velocity at 10 m AGL [$m \cdot s^{-1}$]	Standard deviation [$m \cdot s^{-1}$]	WPD at 10 m AGL [$W \cdot m^{-2}$]
Camarasa	5.75	2.45	186.52
Certascan	3.57	1.9	43.23
Darnius	2.64	1.7	35.04
Oliana	2.25	0.88	9.92

Camarasa is located in west Catalunya, with typical Mediterranean climate [48]. The mountainous area around the dam is mainly covered by low shrubs. The reservoir has a maximum water capacity of 113 hm^3. The 82 m height dam, built in the 1920s, sits on the eastern edge of the reservoir,

connecting the north and south mountainous ridges (see Figure 4). Measured wind data are limited to a single weather station, which cannot be representative of the wind over the entire area due to the complex terrain features. Hence, it is interesting to combine these on-site measurements with CFD simulations to obtain efficient and high-resolution assessment of the local wind resource, especially near the dam.

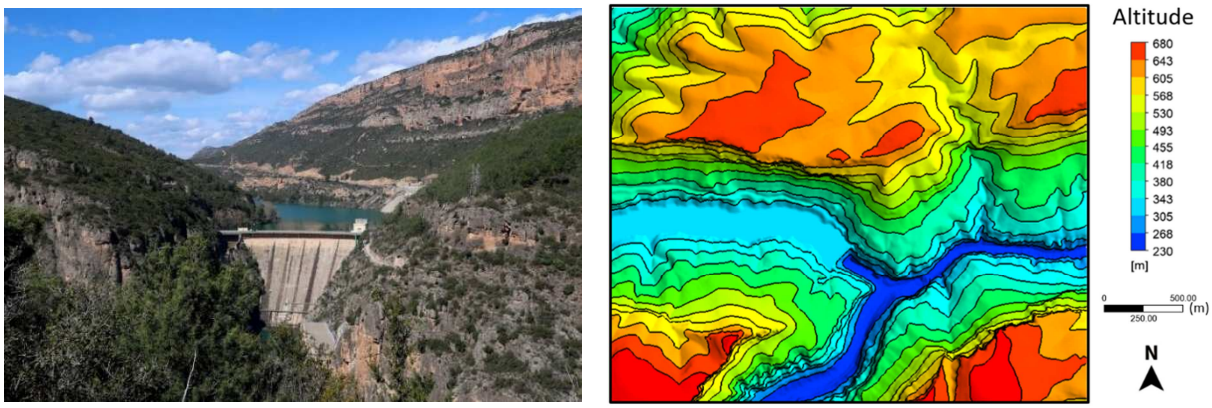

Figure 4. Overview of Camarasa dam [49] (left) and map of altitude [m] ASL of the topography near the dam (right)

Figure 4 (right) shows the altitude above sea level (ASL) of the terrain near Camarasa dam. Accessibility, critical for easy turbine installation and maintenance, can be related to the altitude gradient. Steep terrains can be observed, like the ridges south and south-east (SE) of the dam, and the skirt of the mountain north from the reservoir. Low-slope areas, more favorable to turbine installation, are also found: the ridge north from the dam, and the skirt of the mountain north-east (NE) from it.

MeteoCat's weather station is in the top of the hill located north-west (NW) of the dam (see Figure 5), with coordinates 41°55'04.1"N, 0°52'54.3"E. The surrounding exposure is typically low open shrub land. The station records wind speed and direction data at 2 m AGL, or 646 m ASL. The data used in this study were measured from January 2010 to December 2017 every 30 min. In Section 2.1, Figure 2 (left) displays the obtained annual statistics, with the wind direction classified into 16 equal sections with different weighting factors. The dominant (most frequent and highest speed) wind directions are west, east south-east (ESE), west north-west (WNW), and east, indicating the thermal wind nature of these winds [50], as the valley and reservoir are aligned in the east-west direction between mountainous terrains. Note that choosing a location where thermal winds occur is an advantage, since, as commented in the Introduction, they usually show higher regularity and periodicity, constituting a more reliable and predictable source of wind energy. It thus confirms that the selected area of Camarasa is a good candidate for wind turbine sitting. For comparison purposes, Figure 2 (right) shows wind direction data obtained around Camarasa from the GWA [24] at 50 m

AGL, with geographic resolution of 10 × 10 km^2. The observed discrepancies in the wind roses are due to the fact that MeteoCat's data are limited to measurements at the weather station, at 2 m AGL, whereas the GWA data correspond to a larger grid size at 50 m AGL. However, in both cases dominant wind directions are east and west.

3.2 Topographic CAD of the area of interest and mesh scheme

The topographic model used in this CFD analysis was the Digit Terrain Model (DTM), obtained based on geographic information system (GIS) data. The topography in Figure 5 (right) was downloaded from the Spanish National Centre of Geographic Information (CNIG) database [51], with a resolution of 5 m. Since the interesting area is the one surrounding the dam, the domain for the simulation is defined as a 3.5 km long (in the x-axis) and 3.0 km wide (in the y-axis) parallelepiped, with the dam located in its center. In this model, the reference frame shown in Figure 5 (right) has the x-axis pointing towards east, the y-axis towards north, and the z-axis towards the zenith.

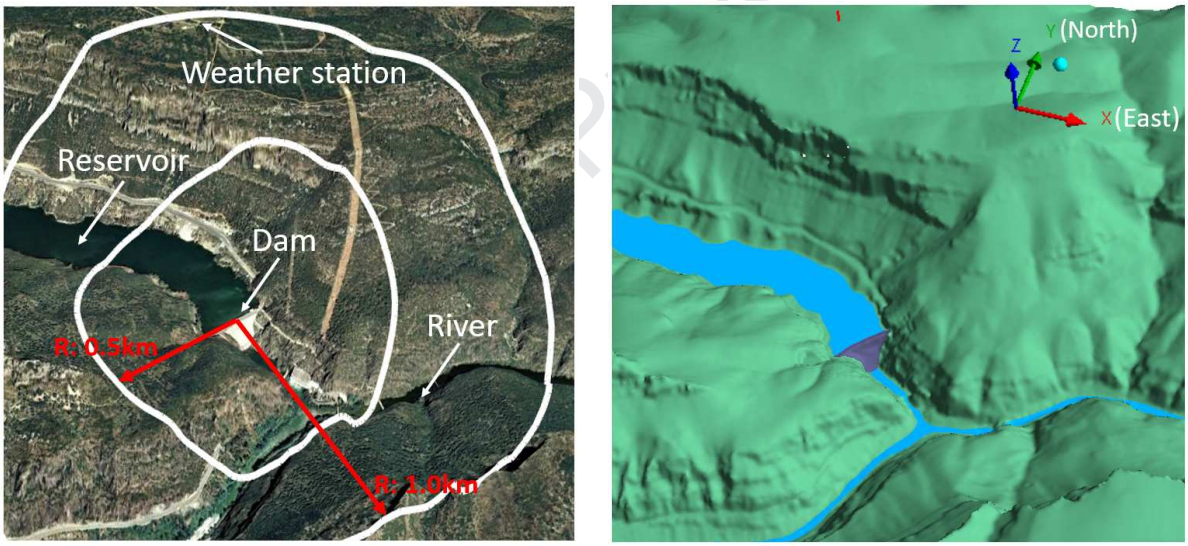

Figure 5. Satellite view of Camarasa dam area (left) and computational model obtained from GIS data (right)

The top boundary of the computational domain is a horizontal plane, with height AGL varying from 350 to 684 m (in the z-axis). According to analysis of field observations [52], as the height AGL is over 300 m everywhere, it has no influence on the accuracy of the CFD results in the interesting area, which is below 40 m. The four lateral boundaries are vertical planes that will serve for setting up inlet and outlet boundary conditions in the CFD simulations described in Section 3.3.

ANSYS ICEM CFD 17.2 software [53] was used for meshing the topography model. Due to the complexity and detailed features of the terrain, triangular elements had to be used on the topography surface, while unstructured tetrahedral elements were used within the computational domain. Around the dam and weather station, a high-resolution mesh is necessary to obtain

accurate results (see Figure 6). To capture the wind speed-up phenomenon, the surface cells are refined at the dam, hilltop, and areas with steep slopes, as seen in Figure 6 (right). Since the resolution of the topographic model obtained from CNIG was 5 m, a body sizing of 2 m was used in the region of interest, whereas a coarser body sizing of 5 m was used around the dam and potential speed-up areas. For the regions far away from the ground, relatively large cells were used to reduce the total number of cells. Within the computational mesh, the coarsest element size was set to 70 m. To precisely predict the ABL flow deceleration and recirculation over hilly terrain, it is imperative to vertically refine the mesh close to the ground [54]. Therefore, an inflation mesh of 8 prism layers was used with a first layer height of 0.2 m, as seen in Figure 6 (left). Satisfactory values of y^+ of between 1 and 5 were obtained on top of the speed-up areas. The total number of cells for the basic mesh set up reached 5.6 million.

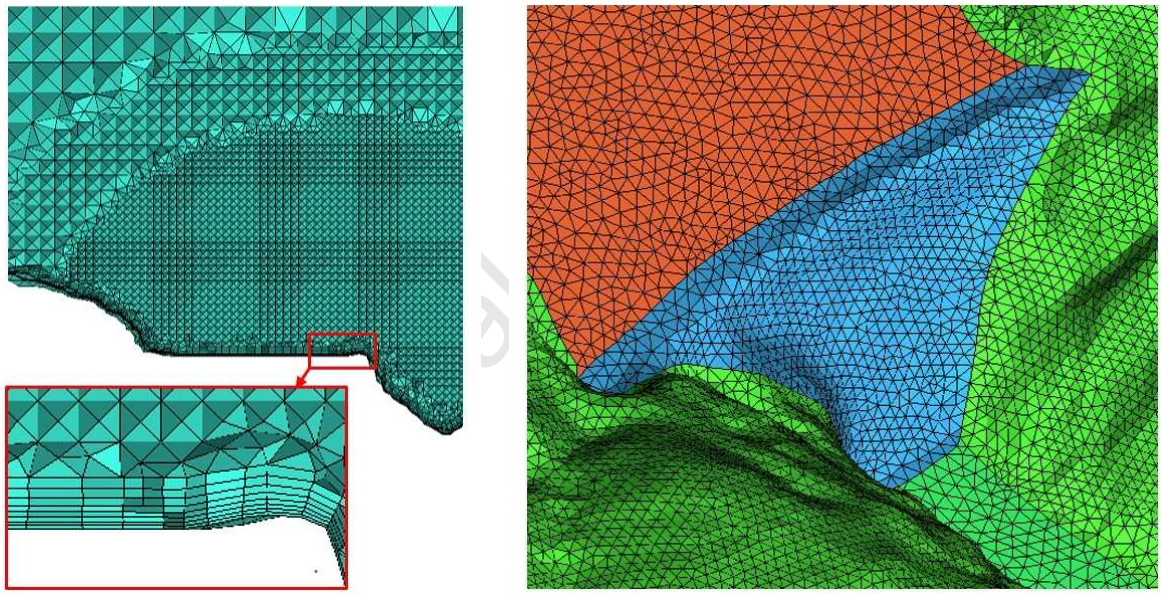

Figure 6. Details of volume meshing near dam (left) and surface meshing near dam (right)

To examine the mesh independence, two additional grid schemes were generated based on the basic grid. A 3.1 million cells coarser grid was obtained by coarsening the basic grid a factor of 1.8. Similarly, a finer grid consisting of 8.9 million cells was generated by refining the basic grid by a factor of 0.75. Numerical simulations using these three grids were performed in the east wind direction (one of the dominant wind directions), and the obtained results were compared. Particularly, the wind speeds in three locations of interest were sampled along the evaluation lines: Location 1 (the dam), Location 2 (the mountain), and Location 3 (the weather station).

Table 2 shows the error of the coarser and basic meshes with respect to the finer mesh for the wind speed at 15 m AGL in these three locations. It is clear that the basic grid has much smaller error compared with the coarser grid and provides a maximum error of 2.3% with respect to the finest

one for these three locations. It was thus concluded that the basic grid provides a good balance between accuracy and computational efficiency for this study.

Table 2. Error in wind speed results at 15 m AGL as obtained from coarser and basic meshes with respect to finer mesh, at three locations: Location 1 (the dam), Location 2 (the mountain), and Location 3 (the weather station)

Mesh	Location 1		Location 2		Location 3	
	Velocity [m·s^{-1}]	Error	Velocity [m·s^{-1}]	Error	Velocity [m·s^{-1}]	Error
Coarse	7.02	8.50%	3.9	6.90%	6.57	6.80%
Basic	7.73	0.80%	4.15	1.00%	6.89	2.30%
Fine	7.67	-	4.19	-	7.05	-

3.3 CFD numerical model

The wind field was solved using the steady, incompressible Navier–Stokes equations, which govern the air flow and transport principles of incompressible turbulent flows using mass and momentum equations. The governing equations were solved using the commercial CFD software ANSYS CFX 17.2 [53], which is based on a coupled finite volume solver. In CFX, the numerical schemes use a co-located grid method to identify the control volume, and a modified Rhie-Chow algorithm for the mass flows to avoid the velocity-pressure decoupling. In governing equations, shape functions are used to evaluate spatial derivatives for all diffusion terms, while the High Resolution Scheme is implemented for the convection term in velocity calculation [55], and a first-order Upwind Differencing scheme is used for the convection term in the turbulence model [53].

The Shear Stress Transport (SST) model was chosen to capture the turbulent flow over hilly terrains. It combines *k*-epsilon and *k*-omega models by applying a blending function method [56]. By adding the transport effects into the formulation of eddy viscosity, this model provides highly accurate predictions of flow separation under adverse pressure gradients, such as the complex terrain around dams. The good performance of this model has been demonstrated in a number of validation studies [21, 57].

The convergence criteria were set such that scaled residuals of all variables fall below 10^{-6}. The numerical simulations of wind flow over Camarasa area were carried out with 16 azimuth sections at a uniform interval of 22.5º. Thus, the CFD simulations represent 16 different wind directions, which are consistent with the weather station data. Each of the presented simulations took approximately 7 hours of computational time running on an 8-parallel-thread, 32 GB RAM computer.

Even though the air density ρ varies with altitude, in the simulations it was considered constant ($\rho = 1.185$ kg/m^3) since the change of altitude in the domain leads to a maximum error of 3.5%, with respect to considering an averaged value. In addition, the following boundary conditions were set

for the numerical simulations: at the inlet of the domain, the logarithmic vertical wind speed profile described in Eq. (3) was applied to account for neutral atmosphere [43]. In the simulation model, the roughness length z_0 was chosen based on the observed topology, i.e., the type of terrain and surrounding obstacles: in accordance with World Meteorological Organization (WMO) specifications [58], the class index for Camarasa is 7, and thus z_0 can be taken as 1 m.

The direction of the inlet velocity was set up based on a Cartesian coordinate system consistent with the local wind direction. For the inlet turbulence, considering the terrain complexity and wind velocity, turbulence with medium intensity of 5% was chosen, with eddy viscosity ratio of 10 [53]. Figure 7 presents the inlet velocity profile for one example: the SE wind scenario. On both south-side and east-side inlet boundaries, the velocity magnitude increases with altitude, satisfying the typical logarithmic vertical profile of the wind speed of Eq. (3).

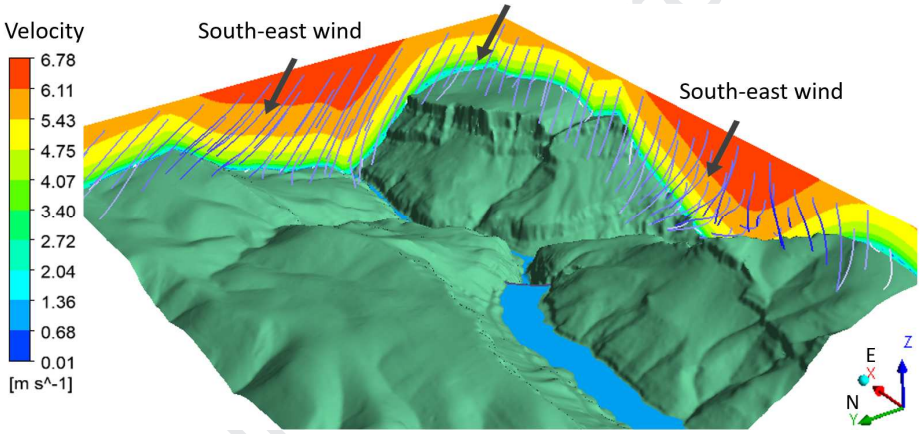

Figure 7. Plot of SE wind inlet velocity setup in the CFD simulation model of the Camarasa area

For the ground, boundary conditions were set as non-slip wall with different roughness values. The area covered with vegetation used a roughness height of 1 m, whereas on the dam the roughness was lowered to 0.05 m, and the river and reservoir were considered as smooth walls. The top boundary condition was set as free-slip wall. Finally, for consistency with the inlet velocity setup, outlet boundaries were set as pressure outlet, with a specified relative pressure of 0 Pa.

From the weather station data, the mean wind profile in Camarasa was presented in 16 directions with different weighting factors, as shown in Figure 2 (left). For coherence with these statistical results, 16 CFD simulation cases were setup to describe all wind scenarios in Camarasa. By considering the weighting factor of each wind direction, the final regional wind profile can then be analysed by post-processing the simulation results of all 16 directions.

To be able to present coherent results anywhere in the computational domain, it is critical to first assess how the local wind direction might change from the one imposed at the inlet of the domain.

Since in this case study measured data are available only at a single point, the procedure followed was to tune the inlet velocity at the boundary such that the simulation results (values of wind speed and direction) at the weather station would match the weather station measurements.

First, CFD results for wind direction at the weather station were compared with inlet wind direction for 8 dominant wind directions, as shown in

Table 3. Note that, in almost all cases, the differences in the directions are smaller than half of the width of the angular sector, i.e., smaller than 11.25º. Thus, the error in change of wind direction between inlet and weather station is within the wind direction error margin. WNW is the only case showing high difference in direction at 10 m AGL (+15.9º), which would correspond to a NW direction. We acknowledge this possible source of error but consider that overall the direction test for inlet tuning is satisfactory, and leave a finer tuning (i.e., considering wind direction more accurately) for future work.

Table 3. Differences between wind direction at the inlet and the weather station (WS) for 8 dominant wind directions

Case	Wind direction at inlet [º]	Wind direction at WS 2 m AGL [º]	Wind direction at WS 10 m AGL [º]	Difference at 2 m AGL [º]	Difference at 10 m AGL [º]
E	90	91.3	93.3	+1.3	+3.3
ESE	112.5	120.4	121.4	+7.9	+8.9
SE	135	137.6	138.5	+2.6	+3.5
SSE	157.5	149.5	154.4	-8.0	-3.1
S	180	177.6	178.4	-2.4	-1.6
WSW	247.5	257.9	257.4	+10.4	+9.9
W	270	276.1	275.4	+6.1	+5.4
WNW	292.5	298.2	308.4	+5.7	+15.9

Then, the velocity magnitude at the inlet boundary condition (V_{inlet}) was tuned for all 16 wind directions: the values of V_{inlet} were set up such that the velocity magnitude obtained from the CFD simulations at the weather station corresponded to the mean velocity at the weather station, as obtained from the MeteoCat measurements.

3.4 CFD results

As previously commented, 16 wind direction cases were simulated separately. The results of each simulation show unique wind flow patterns. To better illustrate this, the four dominant wind directions, i.e., cases E, W, ESE, and south south-east (SSE), are discussed here. Figure 8 shows velocity contours and vortex cores at 10 m AGL for these four scenarios and preliminary candidate locations of interest for turbine sitting. For case E (wind coming from the east and blowing along the valley), relatively high wind velocity is observed over the mountain surface north from the dam. In

addition, over the reservoir, which is west from the dam, high-speed wind is observed, likely due to speed-up effect when the wind moves over the dam. Unlike the other three cases presented in Figure 8, the inlet speed in case W is relatively small. Thus, in general, the wind speed in this case is relative weak in all the domain. However, the wind over the mountainous area north from the dam is still stronger than south from it. In cases ESE and SSE, as the wind is not blowing along the valley, there are strong winds in the area south from the reservoir due to speed-up effect when the wind moves over the mountain in that area. Speed-up effect is also observed at the ridge of the mountain north of the dam. For cases E and W, significant turbulence is observed downwind of the dam, i.e., respectively west and east from the dam. In cases ESE and SSE, significant turbulence is found downwind of the speed-up area over the mountain south from the reservoir.

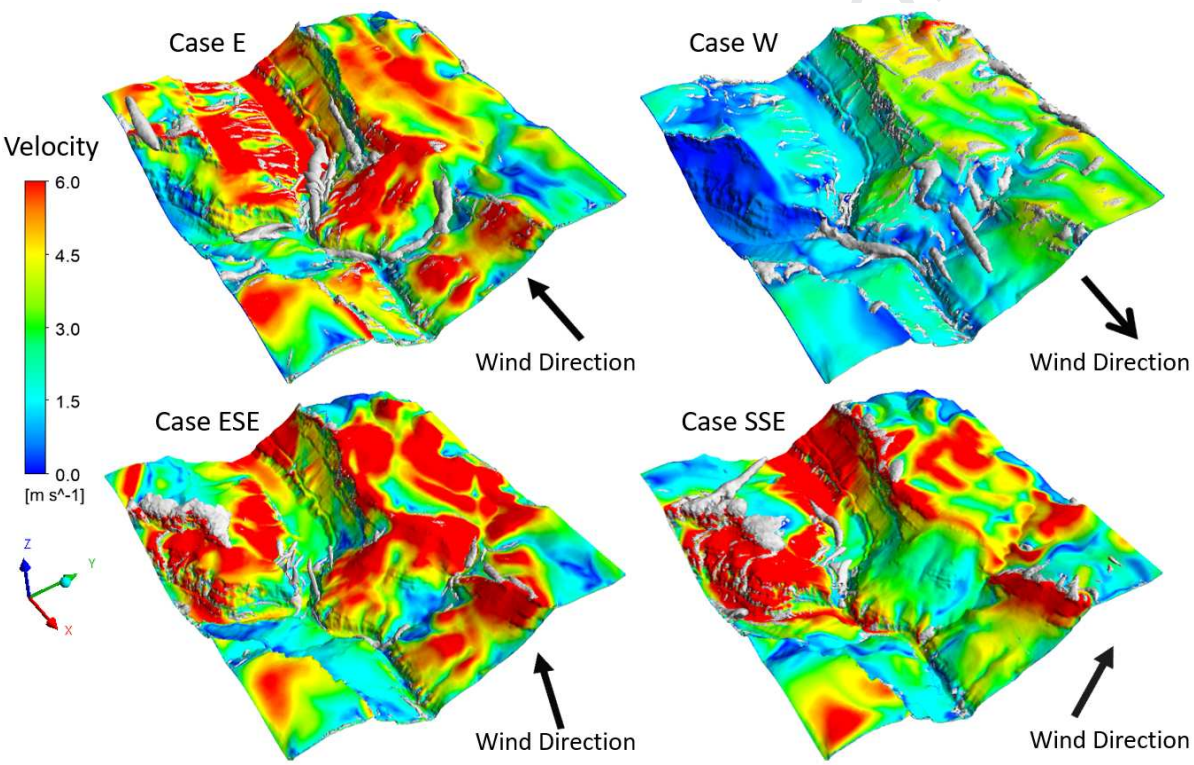

Figure 8. Velocity contours and vortex cores at 10 m AGL for four dominant wind directions in Camarasa area

The wind flow patterns observed in the 16 wind directions are different, in some cases even showing opposite characteristics. To identify suitable sites for installing wind turbines, it is thus necessary to obtain overall wind profiles averaged for a whole year, by creating global velocity and TKE contour maps.

The results of the 16 simulated directions are now combined in a weighted-average wind speed map (see Figure 9), by considering the probability of wind blowing in the corresponding direction, that is, using data similar to the one available from Figure 2. Three areas are now found to have strong wind

speed-up effect: zone 1, the ridges north from the dam; zone 2, the area over the hill south from the reservoir; and zone 3, the skirt of the hill NE from the dam. On the contrary, along the reservoir, the wind velocity is relatively low in general, but might still be used to generate wind energy.

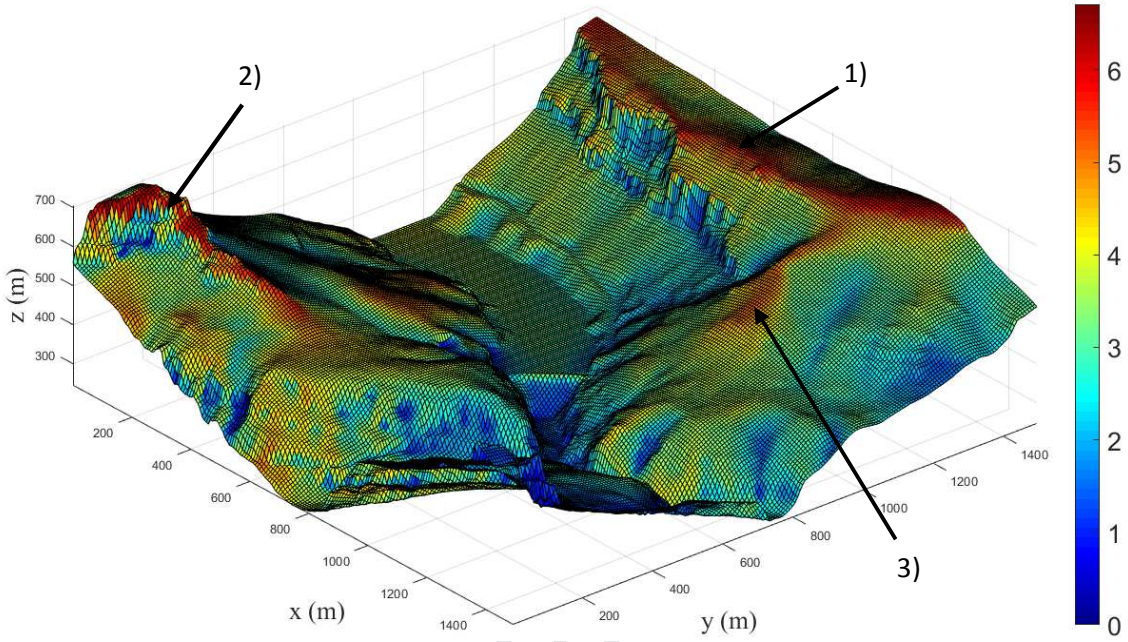

Figure 9. Map of weighted average of wind speed [m·s^{-1}] at 10 m AGL in Camarasa area

Following a similar procedure, a weighted-average TKE map was obtained (see Figure 10). Lower TKE means that the local wind speed profile is more uniform, which is good for wind turbine operation. In contrast, high TKE means more vortices could be developed in the area. It can be seen that relatively high TKE can be found over the hill south from the reservoir (zone 2), because east and west are the dominant wind directions. Besides, in the ridges north from the dam (zone 1), some turbulence is observed in the immediate edge of the hill, which could be expected [21], though not as high as in zone 2. Finally, on the skirt of the hill NE from the dam (zone 3), where relatively high wind speed was observed, TKE is much lower.

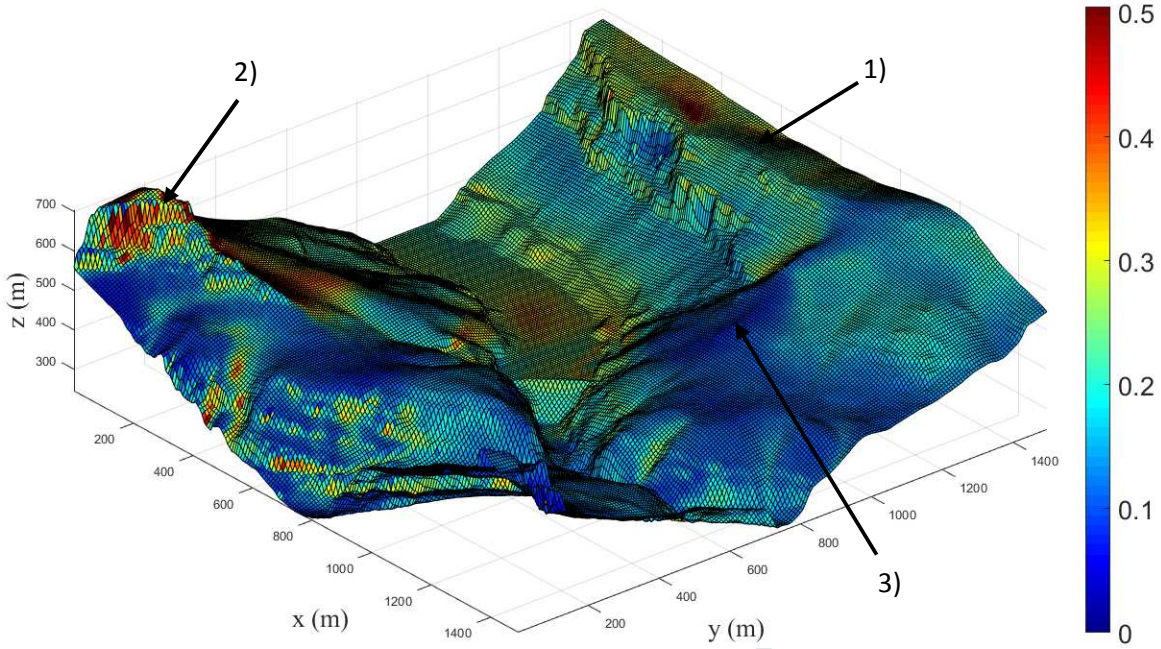

Figure 10. Map of weighted average of turbulence kinetic energy [$m^2 \cdot s^{-2}$] at 10 m AGL in Camarasa area

3.5. Wind energy estimations

Though the weighted-average wind speed map presented in Figure 9 gives valuable information for wind turbine sitting, it only considers annual mean wind speeds, and not the detailed distribution of wind (both in magnitude and direction) along the year. To improve the accuracy of the calculated WPD and annual energy production, a more detailed process is proposed next.

First, the Weibull distribution function is now fitted to the ensemble of wind speeds at the weather station in each wind direction bin (16 direction sectors). A correspondence between the measured wind speed at the weather station and at any other location must then be found. As commented in Section 1, many wind resource assessment studies are based on linearization of the flow motion equations, which show good performance for wind flow description in absence of flow separation, i.e., for low slopes [23]. In the present case, featuring complex terrain with steep slopes, non-linearity of the results can be expected. However, to ascertain whether the obtained wind profile is linear or not with the inlet velocity, a set of tests were conducted at several locations. Particularly, for each wind direction i, more than four different wind velocities have been set at the inlet, and the corresponding velocities obtained from CFD have been evaluated at three different locations. Next, the applied procedure is illustrated for two relevant wind directions.

Figure 11 (left) shows the wind speed at three locations at three different heights AGL (10, 20 and 30 m) for the main wind direction (west). It can be seen that the behaviour of the wind speed is very close to linear. Similar results were obtained for the second main wind direction (east). Errors due to using linear fitting are around 6%, which is an acceptable level of error. This can be explained by the

fact that the wind is mainly directed along the east-west axis, which follows the longitudinal axis of the valley and reservoir. Thus, the main wind flow would not be passing over steep hills, where linearized models are more prone to fail since total or partial/intermittent flow separation may occur when the flow encounters steep slopes [30].

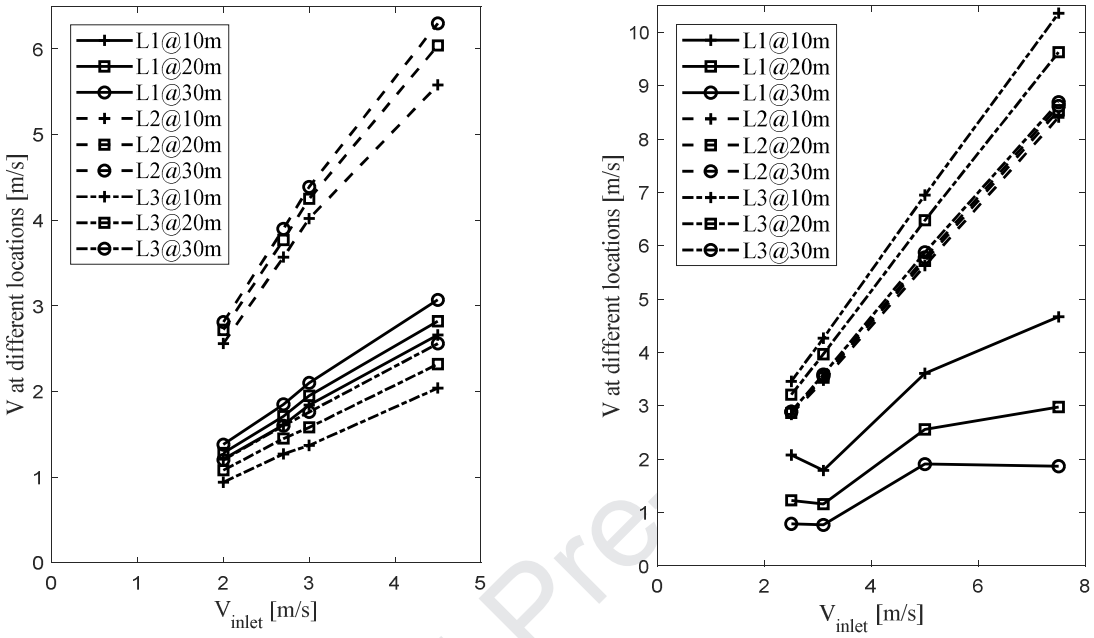

Figure 11. Linearity study for west direction (left) and south direction (right) at height AGL of 10, 20, and 30 m in three locations: Location 1 (the dam), Location 2 (the mountain), and Location 3 (the weather station)

On the contrary, and as expected, Figure 11 (right) shows non-linearity at some locations for a wind direction not aligned with the valley (south). The same non-linearity was also observed in the WSW direction. In these cases, up to 50% of error from a linear behaviour can be observed. Nevertheless, note that non-linearity is observed in wind directions that are among the least frequent ones, and in locations that will probably show higher turbulence, thus anyway these locations would not be adequate for turbine sitting. For these reasons, and for the sake of simplicity as per the proposed global wind resource assessment procedure, overall linearity is assumed in the subsequent analysis, even though we acknowledge that linearity could be a loose approximation in some specific areas. If increased accuracy was necessary, future work should strive to increase the number of simulations when non-linearity is detected, to describe more properly the wind speed at these specific locations.

Based on the hypothesis of linear behaviour of the wind speed, the Weibull distribution function obtained for each point of the grid only differs from the one at the weather station in the scale parameter (the shape parameters are all the same). There is thus no need to make a new Weibull fitting for each grid point. Simply, from the Weibull distribution function for the weather station data, with parameters $\lambda_{i,WS}$ and k_i, the corresponding Weibull function at any location l is obtained using the same shape parameter k_i, and calculating the new scale parameter $\lambda_{i,l} = c_{i,l}\lambda_{i,WS}$. The

proportionality factor $c_{i,l}$ between the wind speed at the weather station and at the location l, for each wind direction i, is obtained from the CFD simulations. Then, the WPD can be calculated at each grid point for each wind direction using:

$$\left.\frac{P}{V}\right|_{i,l} = \frac{1}{2}\rho{\lambda_{i,l}}^3\Gamma\left(1+\frac{3}{k_i}\right) \quad (4)$$

The total WPD is then obtained at each grid point l by multiplying the WPD in each direction times the annual probability p_i of wind blowing in that direction, and then adding the results obtained for the 16 wind directions:

$$Total\ WPD_l = \frac{1}{2}\rho\sum_{i=1}^{16}\lambda_{i,l}^3\Gamma\left(1+\frac{3}{k_i}\right)p_i \quad (5)$$

Table 4 compares, for four different locations, the WPD obtained with Eq. (5), i.e., using 16 adjusted Weibull functions (one for each wind direction), with the WPD obtained using a single global Weibull for all wind directions, i.e., applying the following equation:

$$Total\ WPD_l = \frac{1}{2}\rho\lambda_{WS}^3\Gamma\left(1+\frac{3}{k}\right)\sum_{i=1}^{16}c_{i,l}^3\,p_i \quad (6)$$

Table 4. Wind power density (WPD) at four locations: the dam, NE and SE from the dam, and the weather station

Location	WPD from 16 Weibull distributions [W·m^{-2}] Eq. **(5)**	WPD from 1 Weibull distribution [W·m^{-2}] Eq. **(6)**	Error
LOC 1 (Dam)	81.5	98.1	-16.9%
LOC 2 (NE from dam)	229.7	146.0	57.3%
LOC 3 (SE from dam)	57.72	92.5	-37.6%
LOC 4 (weather station)	145.8	146.0	-0.1%

The last case (LOC 4) corresponds to the weather station, which serves as a reference, since $c_{i,l} = 1$. Thus, both methods for calculating the WPD should yield the same results. However, an error of 0.1% is observed. The difference obtained comes from using 16 Weibull distributions instead of only one Weibull function for all wind directions. Indeed, since for each individual direction there are less data than considering all directions altogether, the Weibull fitting is not as good as with the global data. Nonetheless, the error is extremely small.

On the contrary, for the other three locations, significant differences are obtained, and the WPD obtained using a single Weibull distribution can be either sub- or over-estimated. This can be explained by the fact that, when only a single Weibull function is considered for all wind directions, the analysis does not take into account that some wind directions may be very beneficial for some

sites, which is determined by the value of $c_{i,l}$ (see LOC 2 for example), and these directions may have a high probability of occurrence.

Figure 12 shows the obtained map of WPD. As commented, it serves much better for turbine sitting than considering only the weighted average of wind speed in Figure 9, since it takes into account not only annual mean wind speeds but the Weibull distributions of the wind in each direction. It is important to remark again the key difference between both computations: while Figure 9 uses the same general Weibull distribution for all directions, though each direction should have a different weight depending on the probability of the wind blowing in that direction, Figure 12 uses a distinct Weibull distribution for each of the 16 studied directions, making the results more accurate. Note that, it is still necessary to use Figure 12 together with Figure 10, to avoid areas of high turbulence, where, on top, linearity of the wind speed is less obvious, and to validate the accessibility of the site.

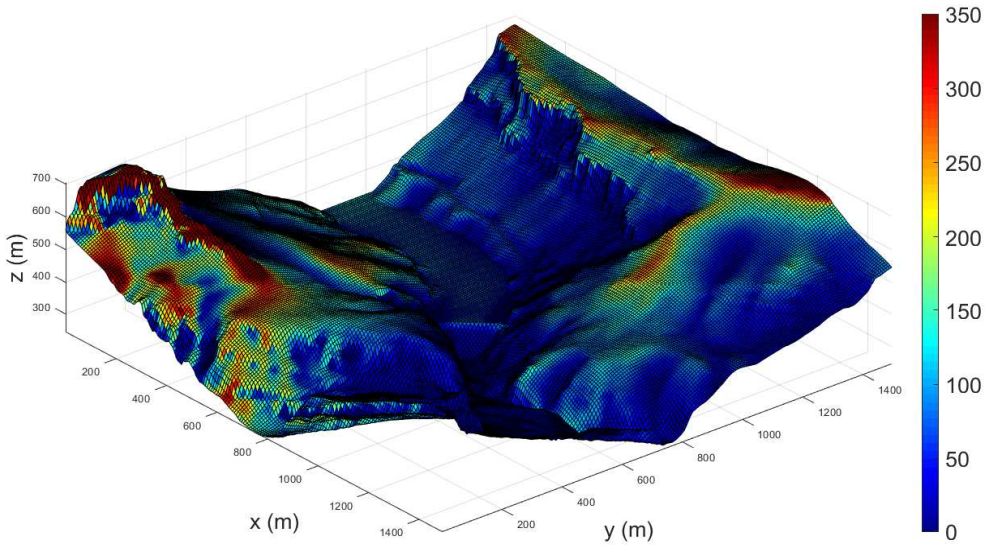

Figure 12. Map of wind power density [W·m^{-2}] at 10 m AGL in Camarasa area

Finally, the annual energy production was estimated using a medium-power wind turbine: the AH-10kW pitch-controlled turbine from the Chinese manufacturer Qingdao Anhua New Energy Equipment (see Figure 13). Table 5 compares the energy results obtained using 16 fitted Weibull distributions with those obtained using a single Weibull function for the data altogether. The results are again quite different for LOC 1 and LOC 3, but not for LOC 2. This can be explained by the fact that a significant percentage of the wind speed was lower than 2.5 m·s^{-1}, which is accounted in WPD, but does not effectively serve to produce energy, since it is lower than the start-up speed of the turbine.

To sum up, Figure 14 shows the final map of potential energy production in the Camarasa area using an AH-10kW turbine. It confirms that the previously identified site, i.e., the skirt of the hill located NE from the dam (zone 3 in Figure 9), would be a viable candidate to install small and medium-power wind turbines.

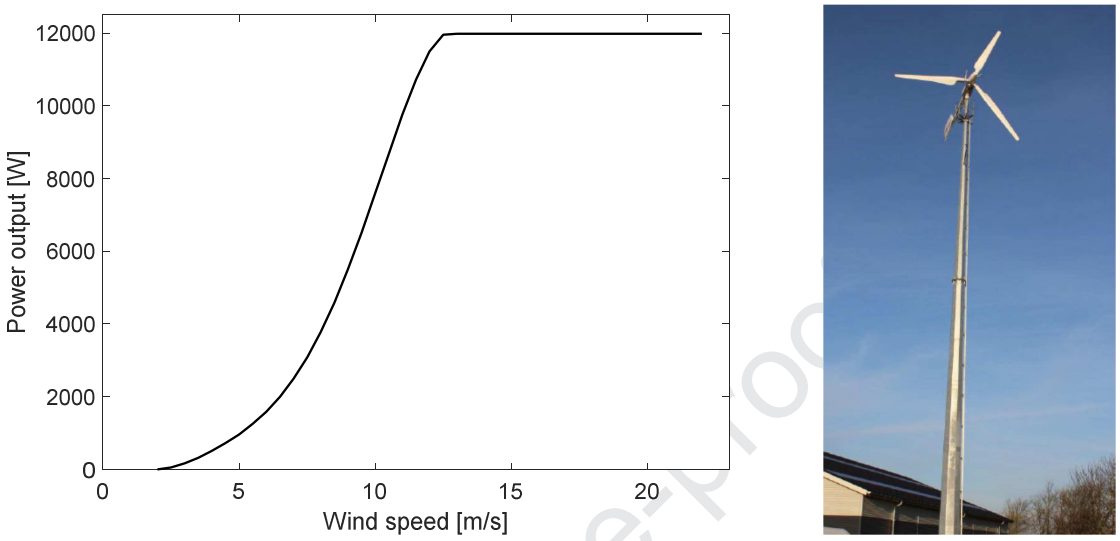

Figure 13. AH-10kW turbine (Qingdao ANE): (left) power curve; (right) wind turbine

Table 5. Annual energy production at four locations using an AH-10kW turbine, with hub-height 10 m

Location	16 Weibull-based annual energy [MWh]	1 Weibull-based annual energy [MWh]	Error
LOC 1 (Dam)	6.3	9.5	-33.7%
LOC 2 (NE from dam)	15.7	14.1	11.3%
LOC 3 (SE from dam)	5.3	8.9	-40.4%
LOC 4 (weather station)	13.7	14.1	-2.8%

3.6 Error estimation and comparison with Wind Atlas and WAsP

As previously discussed, some error has to be accounted in this study due to the mesh and due to using constant density with altitude. The total maximum error obtained in velocity results is estimated around 6%, which we believe is reasonable for this kind of preliminary assessments that do not aim to reach extreme accuracy, but rather aim to reach a good balance between accuracy and efficiency, by limiting the computational time. Then, when linearity is assumed to generate WPD and energy maps, providing further information beyond simple annual mean wind speeds, an extra error is generated highly dependent on the local topography, and thus making very difficult to estimate the global error. As mentioned before, if increased accuracy was necessary in areas where high non-linearity is expected or observed, a finer study on non-linear effects would be required.

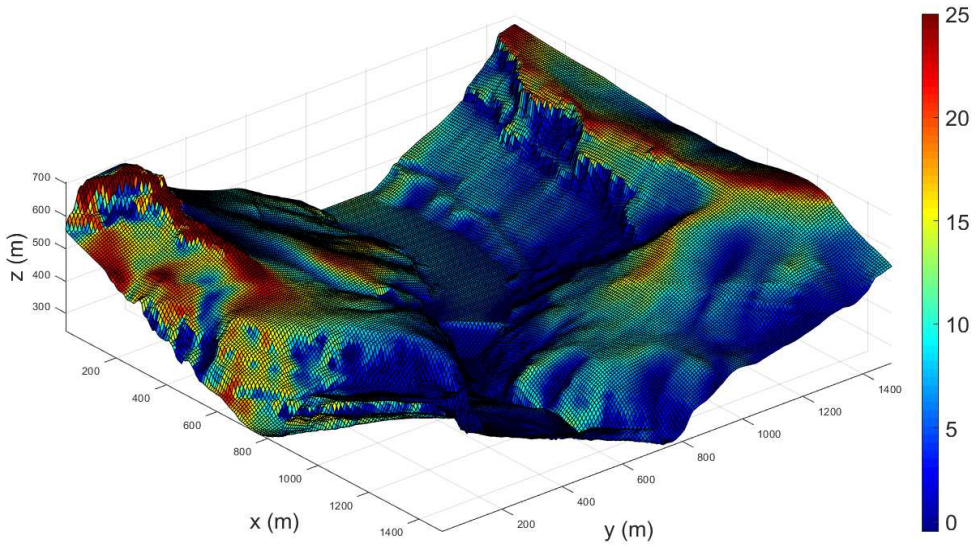

Figure 14. Map of energy [MWh] potentially harvested in Camarasa area with an AH-10kW turbine, with hub-height 10 m

When dealing with results on energy, since it involves the cube of the velocity, any source of error in velocity is greatly amplified. In this regard, we consider that the WPD and energy maps might show a maximum error of around 19%. Although this error is significant, it is important to recall that this is a maximum value, not necessarily occurring in all locations. Moreover, for preliminary assessment purposes, we believe that it still leads to a correct order of magnitude, as well as higher accuracy than if using only GWA data, for example. Indeed, Figure 15 shows the wind speed and WPD obtained from GWA (DTU, 2018) at 50 m AGL. Namely, the wind speed maps shown there do not capture the speed-up effect detected thanks to a finer study. As a consequence, in areas that we identified as suitable for wind turbines (see Figure 9), with an estimated WPD around 300 W·m^{-2}, the GWA prediction is below 100–150 W·m^{-2}, corresponding to a 100–200% difference.

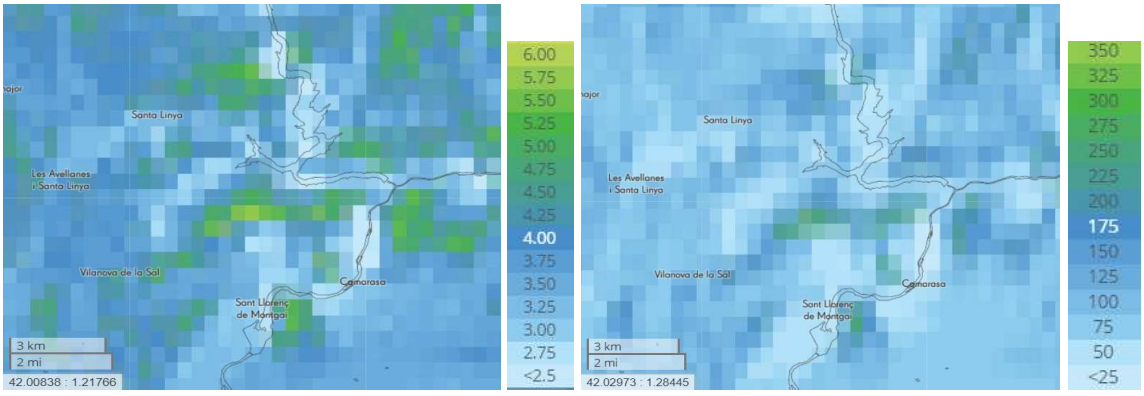

Figure 15. GWA of wind speed [m·s^{-1}] (left) and wind power density [W·m^{-2}] (right) in Camarasa area

The results obtained following the proposed procedure are now also compared with those obtained from conventional linear model simulations using WAsP. WAsP software is commonly used by industry to estimate wind energy resources [59]. The program uses long-term meteorological data series at a reference site to estimate conditions at other predicted sites. To ensure a fair comparison, the setup of the WAsP case here uses identical input data as those used in our methodology, including the Camarasa weather station wind data, the DTM model, and the power curve of the AH-10kW wind turbine generator. Note that, as expected, simulation time for WAsP is less than 1 hour, much faster than the CFD simulation that takes nearly 7 hours each, leading to around 100 hours for all wind directions. Grid resolution also differs since the results of resource-grid in WAsP are calculated based on the grid resolution of 20 m, whereas CFD simulation are based on 2 to 5 m grid. The comparisons of the results (considering all wind directions, at 10m AGL) on wind speed, WPD, and annual energy production are presented in Figure 16.

Figure 16 shows that both methods show the same velocity tendency around the Camarasa dam area. As observed in the CFD simulation, the wind speeds from WAsP simulation at the three zones (1, 2, and 3) marked in Figure 9 are higher than in the surrounding areas, whereas relatively small wind speeds are observed near the valley and reservoir area. Both methods show that the highest wind speeds occur in zone 2. Nevertheless, the maximum wind speed obtained from WAsP (4.3 m/s) is 33.8% lower than that obtained from CFD simulation (6.5 m/s). Similar conclusions can also be drawn from the comparison of the WPD and annual energy production. For both methods, the highest values of WPD and annual energy production are obtained in zone 2 and zone 3, as shown in Figure 16, but they are significantly lower with WAsP than with CFD simulations. From WAsP results, the maximum WPD and energy production in zone 2 are 147 W/m^2 and 13 MWh, respectively. These values are 58% and 48% smaller than the results obtained from our methodology (350 W/m^2 and 25 MWh, respectively).

According to a research by Mortensen, to obtain accurate prediction results, WAsP simulations need the surrounding terrain be sufficiently gentle and smooth to ensure mostly attached flows [60]. Thus, the observed discrepancies in predictions of wind speed, WPD, and annual energy production between WAsP and our approach can be explained by the values of the ruggedness index (RIX), shown in Figure 17. Particularly, due to the complex mountainous topography, the Camarasa area has high RIX values ranging from 20.4% to 30.6%. According to the WAsP User Manual [59], high RIX values can lead to large errors in the flow modelling in WAsP simulations. In reality, turbulence exists near the terrain with high ruggedness, which may induce wind vortexes [61]. Meanwhile, the RIX difference between predicted and reference sites (ΔRIX) ranges from -2.7% to 7.5% in this area. The uneven ΔRIX values make WAsP modelling errors to be significant and unequal [60].

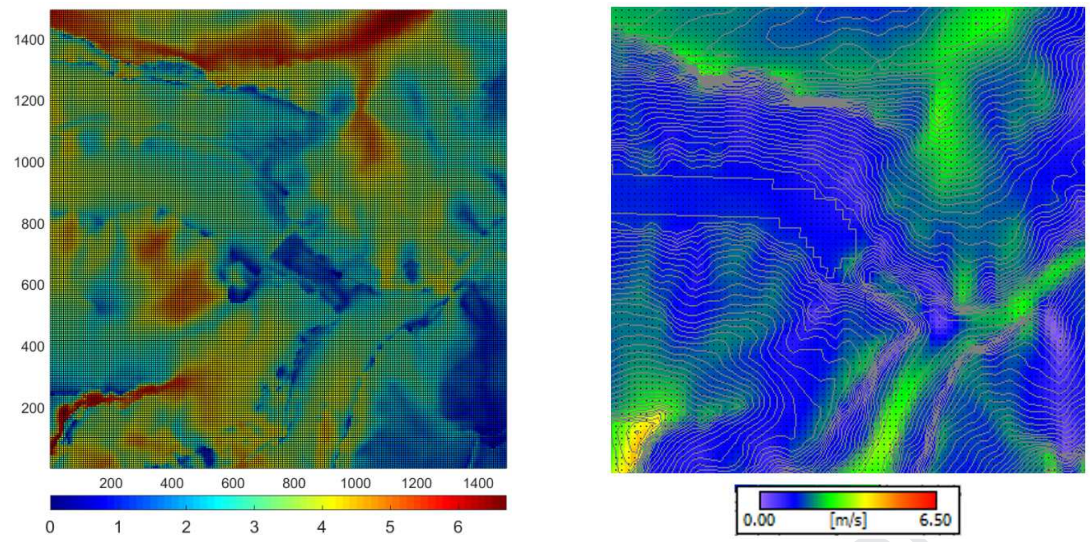

Wind speed [m/s]: CFD (left) vs. WAsP (right)

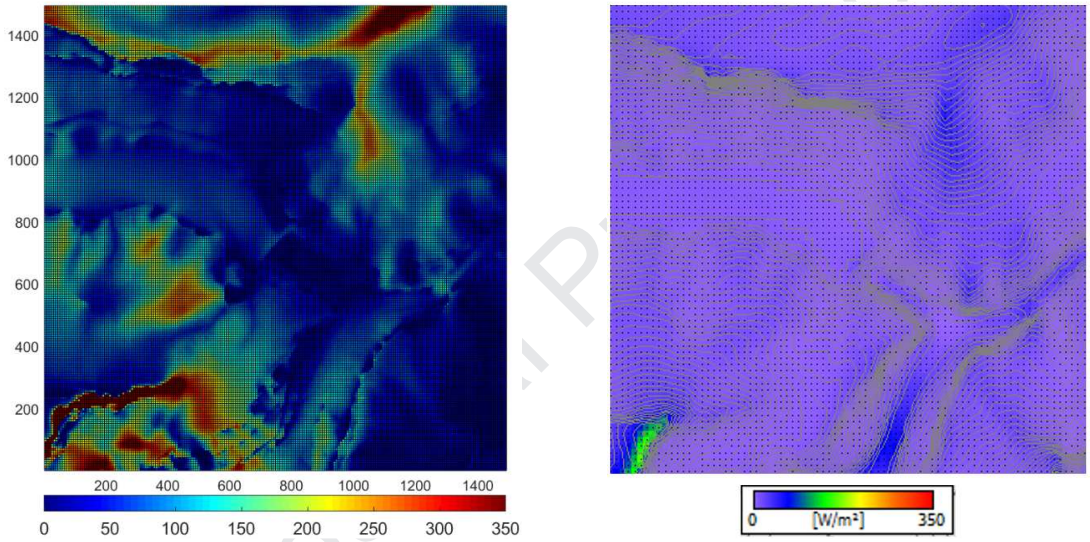

Wind power density (WPD) [W/m^2]: CFD (left) vs. WAsP (right)

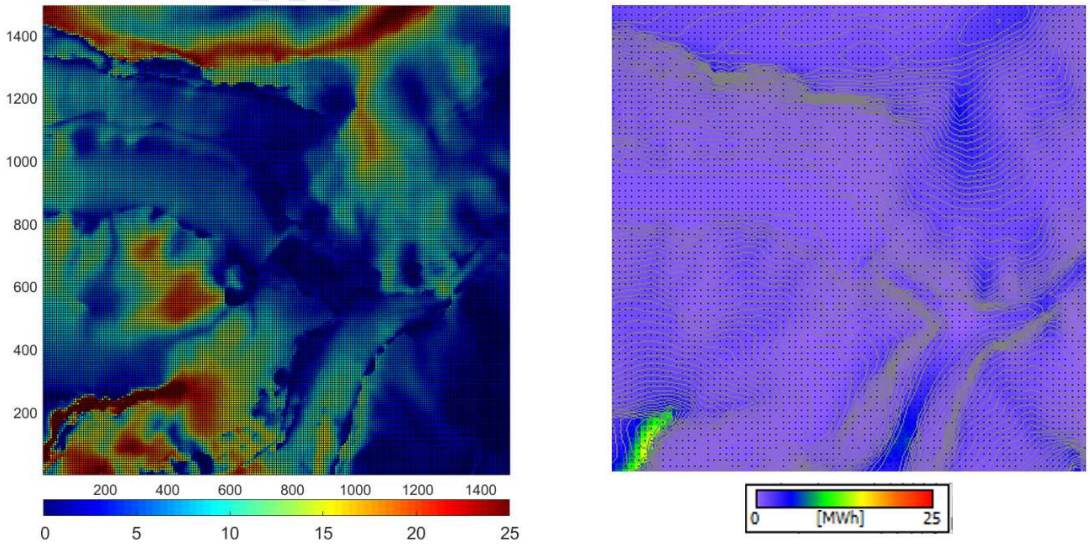

Annual energy production [MWh]: CFD (left) vs. WAsP (right)

Figure 16: Comparisons of results (considering all wind directions, at 10m AGL) obtained following the procedure proposed in this work (left hand side) with those obtained from conventional linear model simulations using WAsP (right hand side): (top) wind speed; (centre) wind power density (WPD); and (bottom) annual energy production.

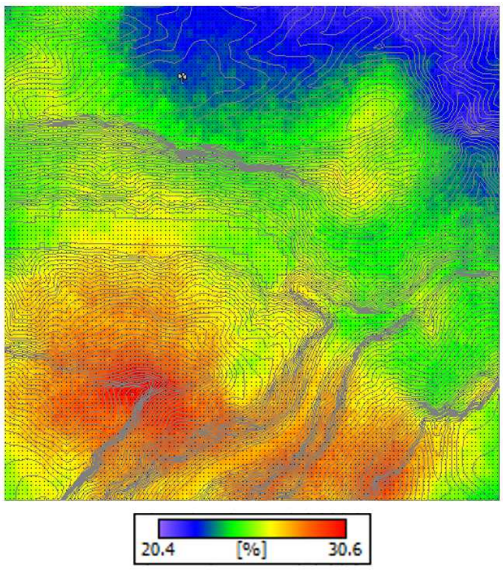

Figure 17 RIX values in Camarasa dam area

Overall, after comparing the results on wind speed, WPD, and annual energy production from the proposed methodology and WAsP, it can be concluded that the results from both methods are consistent: indeed, similar patterns and same orders of magnitude were obtained from both methods, with maximum differences of 33.8%, 58%, and 48% respectively. These differences are considered as acceptable given the high RIX values in the Camarasa area.

3.7 Identification of suitable sites for wind turbines

As discussed in Section 2.4, the selected sites for installing wind turbines should meet the following criteria: 1) be easily accessible; 2) take advantage of speed-up effect; 3) have local uniform incident wind speed profiles; and 4) be close to its paring hydropower dam. Considering all these factors, the skirt of the hill located NE from the dam (zone 3 in Figure 9) is regarded as a good candidate; in this area, the slope is small, while the WPD is high (it appears to effectively take advantage of speed-up effect, as shown in Figure 12), and the annual values of TKE are acceptable. In addition, it is located not far away (less than 500 m) from the dam, as seen in Figure 5 (left). Figure 14 shows that a single turbine in this site would lead to an annual production of around 22 MWh, corresponding to the annual mean electrical consumption of 7 medium Spanish households, and to a carbon footprint saving of 19 and 11 t of CO_2, compared to coal- and gas-obtained electricity, respectively. Note that this turbine model is not very expensive, and the mean payback time of the turbine would be between 2 and 3 years (out of a life expectancy of 20 years), making it profitable in a rather short term.

It is noteworthy that, among the sites identified from Figure 9 to be possible candidates, the north ridge (zone 1) would also be acceptable, although it shows higher turbulence and is located a bit

further from the dam infrastructure. Finally, zone 2 was disregarded due to showing too much turbulence and much worse accessibility (steeper slope), and being much further from the dam.

4. Conclusions and future work

To increase renewable energy generation in hydroelectric dams, a solution is proposed consisting in installing wind turbines close to dams. To facilitate its implementation, we propose a simple procedure for wind resource assessment in complex terrains, which is the typical case near dams. The Camarasa case study is presented to show in detail the steps of our approach. The main conclusions are:

- A wind data statistical study allows easy and quick preliminary selection of candidate sites based on estimated wind power density, and identifies if thermal winds occur.
- The proposed method, combining CFD simulations in the selected locations and statistical analyses, captures properly the main features of the wind (the speed-up effect beneficial to wind energy production, and turbulence and wind shear, which greatly affect turbine performance). This allows to easily identify the most adequate sites considering also accessibility and distance to the dam.
- The method takes into account the detail of wind direction distribution for calculating wind power density, leading to more accurate results than if only mean speeds are used.
- Error estimation and comparison of the results with those of GWA and WAsP simulations validate the proposed method, given the similar flow patterns and orders of magnitude obtained. However, there are still significant discrepancies in wind power density for the Camarasa area, with maximum differences of 200%/58% between the results from GWA/WAsP and those from the proposed method. This suggests limitations of using GWA and/or WAsP for wind resource assessment in areas of complex orography, while the proposed method increases the accuracy of numerical analyses in complex terrains, which is crucial for the successful development of wind farms in such locations.
- The Camarasa case study illustrates how to use general CFD software for wind resource assessment instead of dedicated wind farm design CFD tools. Moreover, it also shows that the method is easy-to-follow, and that, as there is no specific requirement concerning the dam area, it is applicable to any dam. Particularly, considering all the aforementioned factors, the proposed methodology allowed identifying viable sites near the Camarasa dam to install small- to medium-power turbines that would be economically profitable in a rather short term (2 to 3 years): the skirt of the hill located NE from the dam, where the wind power density is 270 $W \cdot m^{-2}$.

As future work, we aim to reduce the sources of error, estimated in the case study to a maximum of 6%/19% for wind speed/WPD. The effect of changing density with altitude could be studied, as well as the non-linearity effects. Economic feasibility assessment could be added to the methodology, and, since the final assessment is based on multiple criteria, a global criteria function defined as a weighted sum of the single criteria could be implemented for use by decision-makers.

It would be interesting to install meteorological masts in relevant locations to obtain experimental data at 10 m height for validation, and to study, in the simulations, the effect of temperature on thermal winds, common in mountainous areas. Moreover, it would be worth analysing the wind resource time fluctuations associated with thermal winds, due to their cyclic diurnal and seasonal fluctuations, often intense during spring and fall, when thermal gradients responsible for these winds are usually largest [62]. Recall that the methodology contemplates identifying thermal winds in the candidate locations, as in the case study, for which the dominant wind directions were aligned with the valley between mountains, indicating a thermal nature of these winds. Furthermore, in the case study, thermal winds are the main contributors to wind energy, but this cannot be generalized to all dams. Nevertheless, the wind nature, synoptic or thermal, does not affect the proposed procedure.

Acknowledgements

The authors thank the financial support provided by the European Union Erasmus + KA107 grant, the Australian Government Research Training Program Scholarship, and the Generalitat de Catalunya grant 2017 SGR 1278.

References

[1] Somot S, Sevault F, Déqué M, Crépon M. 21st century climate change scenario for the Mediterranean using a coupled atmosphere–ocean regional climate model. Global and Planetary Change. 2008;63(2-3):112-26. doi: 10.1016/j.gloplacha.2007.10.003.

[2] IPCC. Climate Change 2007: Synthesis Report - Summary for Policymakers. Valencia, Spain: Intergovernmental Panel on Climate Change (IPCC), 2007.

[3] Vargas-Yáñez M, Moya F, García-Martínez MC, Tel E, Zunino P, Plaza F, et al. Climate change in the Western Mediterranean Sea 1900–2008. Journal of Marine Systems. 2010;82(3):171-6. doi: 10.1016/j.jmarsys.2010.04.013.

[4] Field CB, V.R. Barros, D.J. Dokken, K.J. Mach, M.D. Mastrandrea, T.E. Bilir, et al. IPCC, 2014a: Climate Change 2014: Impacts, Adaptation, and Vulnerability. Part A: Global and Sectoral Aspects. Cambridge, UK: Cambridge University Press; 2014. p. 35-94.

[5] Miller JR, Russell GL. The impact of global warming on river runoff. Journal of Geophysical Research: Atmospheres. 1992;97(D3):2757-64. doi: 10.1029/91JD01700.

[6] Tobin I, Greuell W, Jerez S, Ludwig F, Vautard R, van Vliet MTH, et al. Vulnerabilities and resilience of European power generation to 1.5 °C, 2 °C and 3 °C warming. Environmental Research Letters. 2018;13(4). doi: 10.1088/1748-9326/aab211.

[7] Boßmann T, Staffell I. The shape of future electricity demand: Exploring load curves in 2050s Germany and Britain. Energy. 2015;90:1317-33. doi: 10.1016/j.energy.2015.06.082.

[8] Reyers M, Moemken J, Pinto JG. Future changes of wind energy potentials over Europe in a large CMIP5 multi-model ensemble. International Journal of Climatology. 2016;36(2):783-96. doi: 10.1002/joc.4382.

[9] Tobin I, Vautard R, Balog I, Bréon F-M, Jerez S, Ruti PM, et al. Assessing climate change impacts on European wind energy from ENSEMBLES high-resolution climate projections. Climatic Change. 2014;128(1-2):99-112. doi: 10.1007/s10584-014-1291-0.

[10] Wohland J, Omrani NE, Keenlyside N, Witthaut D. Significant multi-decadal variability of German wind energy generation. Wind Energy Science Discussions. 2019:1-21. doi: 10.5194/wes-2019-8.

[11] Karnauskas KB, Lundquist JK, Zhang L. Southward shift of the global wind energy resource under high carbon dioxide emissions. Nature Geoscience. 2017;11(1):38-43. doi: 10.1038/s41561-017-0029-9.

[12] Nogueira M, Soares PMM, Tomé R, Cardoso RM. High-resolution multi-model projections of onshore wind resources over Portugal under a changing climate. Theoretical and Applied Climatology. 2018. doi: 10.1007/s00704-018-2495-4.

[13] Chrust MF, Whiteman CD, Hoch SW. Observations of Thermally Driven Wind Jets at the Exit of Weber Canyon, Utah. Journal of Applied Meteorology and Climatology. 2013;52(5):1187-200. doi: 10.1175/jamc-d-12-0221.1.

[14] Pérez-Foguet A. Characterization of local wind patterns in complex mountain valleys. International Journal of Climatology. 2014;34(6):1741-59. doi: 10.1002/joc.3798.

[15] Poulos G, Zhong S. An Observational History of Small-Scale Katabatic Winds in Mid-Latitudes. Geography Compass. 2008;2(6):1798-821. doi: 10.1111/j.1749-8198.2008.00166.x.

[16] Pagès M, Miró JR. Determining temperature lapse rates over mountain slopes using vertically weighted regression: a case study from the Pyrenees. Meteorological Applications. 2009;17:53-63. doi: 10.1002/met.160.

[17] Stiperski I, Kavčič I, Grisogono B, Durran DR. Including Coriolis effects in the Prandtl model for katabatic flow. Quarterly Journal of the Royal Meteorological Society. 2007;133(622):101-6. doi: 10.1002/qj.19.

[18] Blanco MI. The economics of wind energy. Renewable and Sustainable Energy Reviews. 2009;13(6-7):1372-82. doi: 10.1016/j.rser.2008.09.004.

[19] Dhunny AZ, Lollchund MR, Rughooputh SDDV. Wind energy evaluation for a highly complex terrain using Computational Fluid Dynamics (CFD). Renewable Energy. 2017;101:1-9. doi: 10.1016/j.renene.2016.08.032.

[20] Yli-Hannuksela J. The transmission line cost calculation. Jyväskylä, Finland: University of Applied Sciences, 2011.

[21] Montlaur A, Cochard S, Fletcher DF. Formation of tip-vortices on triangular prismatic-shaped cliffs. Part 2: A computational fluid dynamics study. Journal of Wind Engineering and Industrial Aerodynamics. 2012;109:21-30. doi: 10.1016/j.jweia.2012.06.004.

[22] Cochard S, Letchford CW, Earl TA, Montlaur A. Formation of tip-vortices on triangular prismatic-shaped cliffs Part 1: A wind tunnel study. Journal of Wind Engineering and Industrial Aerodynamics. 2012;109:9-20. doi: 10.1016/j.jweia.2012.06.003.

[23] Palma JMLM, Castro FA, Ribeiro LF, Rodrigues AH, Pinto AP. Linear and nonlinear models in wind resource assessment and wind turbine micro-siting in complex terrain. Journal of Wind Engineering and Industrial Aerodynamics. 2008;96(12):2308-26. doi: 10.1016/j.jweia.2008.03.012.

[24] DTU. Gloval Wind Atlas 2.0. Denmark: Technical University of Denmark; 2018.

[25] Kalverla P, Steeneveld G-J, Ronda R, Holtslag AAM. Evaluation of three mainstream numerical weather prediction models with observations from meteorological mast IJmuiden at the North Sea. Wind Energy. 2019;22(1):34-48. doi: 10.1002/we.2267.

[26] Olsen BT, Hahmann AN, Sempreviva AM, Badger J, Jørgensen HE. An intercomparison of mesoscale models at simple sites for wind energy applications. Wind Energy Science. 2017;2(1):211-28. doi: 10.5194/wes-2-211-2017.

[27] Gasset N, Landry M, Gagnon Y. A Comparison of Wind Flow Models for Wind Resource Assessment in Wind Energy Applications. Energies. 2012;5(11):4288-322. doi: 10.3390/en5114288.

[28] Ayotte KW, Hughes DE. Observations of boundary-layer wind-tunnel flow over isolated ridges of varying steepness and roughness. Boundary-Layer Meteorology. 2004;112(3):525-56. doi: 10.1023/b:Boun.0000030663.13477.51.

[29] Arteaga-López E, Ángeles-Camacho C, Bañuelos-Ruedas F. Advanced methodology for feasibility studies on building-mounted wind turbines installation in urban environment: Applying CFD analysis. Energy. 2019;167:181-8. doi: 10.1016/j.energy.2018.10.191.

[30] Troen I, Hansen BO. Wind resource estimation in complex terrain: Prediction skill of linear and nonlinear micro-scale models. AWEA Windpower Conference & Exhibition. Orlando, FL, United States 2015.

[31] Landberg L, Myllerup L, Rathmann O, Petersen EL, Jørgensen BH, Badger J, et al. Wind Resource Estimation-An Overview. Wind Energy. 2003;6(3):261-71. doi: 10.1002/we.94.

[32] Ferrer E, Montlaur A. CFD for Wind and Tidal Offshore Turbines. 1st ed. Switzerland: Springer International Publishing, 2015.

[33] Horcas SG, Debrabandere F, Tartinville B, Hirsch C, Coussement G. Rotor-tower interactions of DTU 10MW reference wind turbine with a non-linear harmonic method. Wind Energy. 2017;20(4):619-36. doi: 10.1002/we.2027.

[34] Kalmikov A, Dupont G, Dykes K, Chan CP. Wind power resource assessment in complex urban environments: MIT campus case-study using CFD Analysis. AWEA 2010 Windpower. Dallas, Texas, USA 2010.

[35] Yan BW, Li QS. Coupled on-site measurement/CFD based approach for high-resolution wind resource assessment over complex terrains. Energy Conversion and Management. 2016;117:351-66. doi: 10.1016/j.enconman.2016.02.076.

[36] Ha T, Lee I-b, Kwon K-s, Lee S-J. Development of a micro-scale CFD model to predict wind environment on mountainous terrain. Computers and Electronics in Agriculture. 2018;149:110-20. doi: 10.1016/j.compag.2017.10.014.

[37] Polanco G, Muhammad SV. Numerical Study of Wind Resource Assessment of a Complex Terrain. Wind Engineering. 2014;38(2):139-46. doi: 10.1260/0309-524x.38.2.139.

[38] Yang X, Pakula M, Sotiropoulos F. Large-eddy simulation of a utility-scale wind farm in complex terrain. Applied Energy. 2018;229:767-77. doi: 10.1016/j.apenergy.2018.08.049.

[39] Sessarego M, Shen W, van der Laan M, Hansen K, Zhu W. CFD Simulations of Flows in a Wind Farm in Complex Terrain and Comparisons to Measurements. Applied Sciences. 2018;8(5). doi: 10.3390/app8050788.

[40] Castellani F, Astolfi D, Burlando M, Terzi L. Numerical modelling for wind farm operational assessment in complex terrain. Journal of Wind Engineering and Industrial Aerodynamics. 2015;147:320-9. doi: 10.1016/j.jweia.2015.07.016.

[41] Ayala M, Maldonado J, Paccha E, Riba C. Wind Power Resource Assessment in Complex Terrain: Villonaco Case-study Using Computational Fluid Dynamics Analysis. Energy Procedia. 2017;107:41-8. doi: 10.1016/j.egypro.2016.12.127.

[42] Tang X-Y, Zhao S, Fan B, Peinke J, Stoevesandt B. Micro-scale wind resource assessment in complex terrain based on CFD coupled measurement from multiple masts. Applied Energy. 2019;238:806-15. doi: 10.1016/j.apenergy.2019.01.129.

[43] Blocken B, Van der Hout A, Dekker J, Weiler O. CFD simulation of wind flow over natural complex terrain: Case study with validation by field measurements for Ria de Ferrol, Galicia, Spain. Journal of Wind Engineering and Industrial Aerodynamics. 2015;147:43-57. doi: 10.1016/j.jweia.2015.09.007.

[44] Burton T, Sharpe D, Jenkins N, Bossanyi E. Wind Energy Handbook. 1st ed. Chichester, UK: John Wiley & Sons, Ltd., 2001.

[45] Hennessey JP. Some Aspects of Wind Power Statistics. Journal of Applied Meteorology. 1977;16(2):119-28. doi: 10.1175/1520-0450(1977)016<0119:Saowps>2.0.Co;2.

[46] Carta JA, Ramírez P, Velázquez S. A review of wind speed probability distributions used in wind energy analysis. Renewable and Sustainable Energy Reviews. 2009;13(5):933-55. doi: 10.1016/j.rser.2008.05.005.

[47] Meteo.cat. Automatic Weather Stations (XEMA). Barcelona, Spain: Servei Meteorològic de Catalunya; 2018.

[48] Blanco A, Segura I, Cavalaro SHP, Chinchón-Payá S, Aguado A. Sand-Cement Concrete in the Century-Old Camarasa Dam. Journal of Performance of Constructed Facilities. 2016;30(4). doi: 10.1061/(asce)cf.1943-5509.0000823.

[49] Miro A. Ermita Sant Jordi de Camarasa (Serra Carbonera). 2018.

[50] Markowski P, Richardson Y. Thermally Forced Winds in Mountainous Terrain. Mesoscale Meteorology in Midlatitudes. 1st ed. Chichester, UK: John Wiley & Sons, Ltd.; 2010.

[51] CNIG. Digital Elevation Models. Mardrid, Spain: Centro Nacional de Información Geográfica (CNIG); 2018.

[52] Baidya Roy S, Traiteur JJ. Impacts of wind farms on surface air temperatures. Proc Natl Acad Sci U S A. 2010;107(42):17899-904. doi: 10.1073/pnas.1000493107.

[53] ANSYS. ANSYS Manuals. 17.2 ed. Pittsburgh, US: ANSYS, Inc., 2016.

[54] Prospathopoulos J, Voutsinas SG. Implementation Issues in 3D Wind Flow Predictions Over Complex Terrain. Journal of Solar Energy Engineering. 2006;128(4). doi: 10.1115/1.2346702.

[55] Barth T, Jespersen D. The design and application of upwind schemes on unstructured meshes. 27th Aerospace Sciences Meeting. Reno, NV, United States: American Institute of Aeronautics and Astronautics; 1989.

[56] Menter FR. Two-equation eddy-viscosity turbulence models for engineering applications. AIAA Journal. 1994;32(8):1598-605. doi: 10.2514/3.12149.

[57] Bardina JE, Huang PG, Coakley TJ. Turbulence Modeling Validation, Testing, and Development. NASA Technical Memorandum. Moffett Field, CA, United States: NASA Ames Research Center; 1997.

[58] WMO. Guide to Meteorological Instruments and Methods of Observation. Switzerland: World Meteorological Organization, 2008.

[59] Mortensen NG, Heathfield DN, Rathmann O, Nielsen M. Wind Atlas Analysis and Application Program: WAsP 10 Help Facility. Roskilde, Denmark: DTU Wind Energy, 2011.

[60] Mortensen NG, Bowen AJ, Antoniou I. Improving WAsP predictions in (too) complex terrain. European Wind Energy Assiciation (EWEA). Brussels: EWEA; 2006.

[61] Rowcroft J, Burton D, Blackburn HM, Sheridan J. Siting Wind Turbines Near Cliffs: The Effect of Ruggedness. Journal of Fluids Engineering. 2018;141(3). doi: 10.1115/1.4041231.

[62] Mazon J, Rojas JI, Jou J, Valle A, Olmeda D, Sanchez C. An assessment of the sea breeze energy potential using small wind turbines in peri-urban coastal areas. Journal of Wind Engineering and Industrial Aerodynamics. 2015;139:1-7. doi: 10.1016/j.jweia.2015.01.002.

Research Highlights:

- A low-cost methodology to install wind turbines close to dams is proposed
- The proposed locations benefit from wind speed-up effect and thermal winds
- The easy-to-follow methodology combines statistical wind data with CFD simulation
- Case study shows the effectiveness of the methodology and provides error estimation